Elastic scattering from cubic lattice systems with paracrystalline distortion

Hideki Matsuoka,* Hideaki Tanaka, Takeji Hashimoto, and Norio Ise
Department of Polymer Chemistry, Kyoto University, Kyoto 606, Japan
(Received 12 December 1986)

The three-dimensional paracrystalline lattice factors $Z(q)$'s for a face-centered-cubic lattice and a body-centered-cubic lattice, in addition to a simple-cubic lattice, were calculated. The $Z(q)$'s thus calculated could reproduce the diffraction peaks at the characteristic positions for each cubic lattice system over a fairly wide range of g values (g is the degree of the paracrystalline distortion). In addition to the paracrystalline distortion, the thermal oscillation and crystal size effects were also considered. The numerically calculated profiles were compared with light and small-angle neutron scattering curves for polymer latex dispersions and with small-angle x-ray scattering curves for block copolymer films for quantitative determination of the ordered cubic systems.

I. INTRODUCTION

The paracrystal theory for the diffraction pattern and the distribution function $h(r)$ for one-dimensional crystals containing a distortion of the second kind was first proposed by Hosemann.[1] The theory was based on a convolution-polynomial operation, was extended later to two-dimensional cases and has been mainly applied to the determination of the fiber structure.[2] For three-dimensional cases, Steffen and Hosemann calculated the function $h(r)$ and compared it with experimental data for liquid lead.[3] Because of some uncertainties such as the termination effect[4] involved in the procedure for obtaining $h(r)$ from an experimental scattering curve, direct comparison of theoretical and experimental scattering curves [not $h(r)$] seems more appropriate.

We have calculated the lattice factor $Z(q)$ for randomly oriented three-dimensional cubic lattice systems with paracrystalline distortion of the second kind, such as the simple cubic (sc) lattice, the face-centered-cubic (fcc) lattice, and the body-centered-cubic (bcc) lattice. We believe that this three-dimensional theory is useful for the determination of the structure and the degree of distortion of the structure for three-dimensionally ordered systems.

Colloidal particles such as polymer latex and synthetic and biological macroions form an ordered structure in solutions.[5-7] In the case of latex suspensions, scattering profiles have been analyzed by Luck *et al.*[8] Ordering phenomena in such systems has been almost unequivocally proven by ultramicroscopy.[9] Recently, the crystal structure was identified using pseudo[10] and intrinsic[11] Kossel line analyses: According to Yoshiyama *et al.*,[11] bcc structures are stable at low concentrations whereas fcc structures are favored in concentrated regions. By using a cinematographic method, the particles forming the ordered structure were demonstrated to be different from free particles, because the root-mean-square displacement of the free latex particles was very close to the prediction of the Einstein theory on Brownian motion,[12-14] whereas that of the particles in the ordered state was practically zero for a reasonably long period of time (e.g., 30 sec). This observation convinced us of the existence of more-or-less distorted latticelike distributions of the latex particles in dilute suspensions. These experimental facts on "visible" latex suspension appear to support our conclusion that synthetic and biological "invisible" macroions likewise form latticelike ordered structures in dilute solutions, probably with a much larger degree of distortion than in the case of latex particles because of the difference in the geometrical size.

Recently, spherical microdomains of block polymers in bulk and in solutions have been reported to be arranged in an ordered manner with cubic symmetry.[15-19] The symmetry of ordered structures called "superlattices"[19] was in some cases discussed qualitatively on the basis of volumetric considerations, that is, from the peak positions of the scattering maxima observed in the small-angle x-ray scattering (SAXS) and neutron scattering (SANS) from the block polymers: It would be possible to estimate the nearest-neighbor distance D between the spherical microdomains, e.g., A spheres when A-block chains form A-spherical microdomains, and the radius R_A of the A spheres. Comparison of the stoichiometric volume of an A block chain with a volume fraction of A spheres estimated from the experimental values of D and R_A for a given symmetry made it possible to determine the symmetry of the cubic superlattice.[16,18] The relative peak position of the scattering maxima gave additional information on the lattice symmetry.[15,16,18,19] However, no attempts[20] have been made so far to utilize whole scattering curves, such as peak heights and linewidths of the scattering maxima and their positions, for quantitative determination of the symmetry, despite the fact that there is rich information associated with the scattering profiles as shown in Fig. 9, for example. A quantitative determination of the symmetry and its distortion may be made possible by comparison of the experimental profiles with the theoretical profiles for paracrystals with the cubic symmetries, and this is one of the main objects of this paper. The force stabilizing the superlattice[19] and the degree of order

typically existing in the systems have been described elsewhere.[15,16,18,19]

Thus it would be interesting to analyze the nature of the ordered structures, particularly their distortion, and the diffraction patterns of scattered radiation from such distorted structures in terms of the three-dimensional paracrystal theory. We are fully aware of some adverse criticism of the paracrystalline treatment in the three-dimensional cases,[21] but we believe that the paracrystal theory is one of the most convenient methods for elucidating, though approximately, the symmetry of the cubic lattice and the distortion of the ordered structures in question. As examples of the applications, we discuss here the two cubic systems, block polymers and colloidal suspensions, although the physical origins of the ordering[7,19] are distinctly different.

II. THEORY

A. Review of general paracrystal theory

Generally, the scattering intensity $I(\mathbf{q})$ from a paracrystal with a given orientation to a reference axis is given by[1]

$$I(\mathbf{q})=N(\langle|f_0|^2\rangle-|\langle f_0\rangle|^2)+N|\langle f_0\rangle|^2[1-D(\mathbf{q})^2]+(1/v)|\langle f_0\rangle|^2D(\mathbf{q})^2Z(\mathbf{q})\circ[\Sigma(\mathbf{q})]^2 , \quad (1)$$

where $\mathbf{q}$ is the scattering vector, N the number of particles in the paracrystal, $f_0=f_0(\mathbf{q})$ the structure amplitude of the particle, v the volume available per particle, $Z(\mathbf{q})$ the paracrystal lattice factor (associated with the distortion of the second kind[1]), and $\Sigma(\mathbf{q})$ the shape amplitude of the paracrystal. The angular brackets $\langle\ \rangle$ designate an average with respect to distributions of particle size, density, and orientation (in the case when the particle is asymmtrical). The symbol $f\circ g$ designates a convolution,

$$f\circ g(\mathbf{r})=\int d\mathbf{u}\, f(\mathbf{u})g(\mathbf{r}-\mathbf{u}) . \quad (2)$$

The factor $D(\mathbf{q})^2$ represents the thermal vibration of the particles (the distortion of the first kind[1]) about the paracrystalline lattice points.

When the particles are identical and spherical, the thermal vibrations are not significant, and the size of the paracrystal is infinitely large, then Eq. (1) is reduced to

$$I(\mathbf{q})=N|f_0|^2Z(\mathbf{q}) . \quad (3)$$

We define here the three fundamental lattice vectors $\mathbf{a_k}$ for the ideal perfect lattice. The distortion of the lattice points from the ideal lattice points is described by the displacement of the lattice vector $\Delta\mathbf{a_k}$ from $\mathbf{a_k}$. We assume that in a given direction of the lattice the nearest-neighbor distortions are independent and the distortions in three directions are also independent. Furthermore, in this paper the distortion is assumed to be isotropic and given by a Gaussian distribution with a standard deviation Δa_k, although the distortion is generally anisotropic and $\Delta\mathbf{a_k}$ a tensor quantity.

In this case, the lattice factor $Z(\mathbf{q})$ for three-dimensional paracrystals is generally given by[1]

$$Z(\mathbf{q})=\prod_{k=1}^{3}Z_k(\mathbf{q}) , \quad (4a)$$

$$Z_k(\mathbf{q})=\mathrm{Re}\left[\frac{1+F_k(\mathbf{q})}{1-F_k(\mathbf{q})}\right]=\frac{1-|F_k|^2}{1-2|F_k|\cos(\mathbf{a_k}\cdot\mathbf{q})+|F_k|^2} , \quad (4b)$$

$$F_k(\mathbf{q})=|F_k(\mathbf{q})|\exp(-i\mathbf{q}\cdot\mathbf{a_k}) , \quad (5)$$

$$|F_k(\mathbf{q})|=\exp(-\tfrac{1}{2}\Delta a_k^2q^2) . \quad (6)$$

When the paracrystals have an orientation distribution, the observed intensity distribution in one direction I_{obs} is obtained by averaging $I(\mathbf{q})$ in Eq. (1) over all possible orientations:

$$I_{\mathrm{obs}}(q)=\langle I(\mathbf{q})\rangle_{\mathrm{orient}} , \quad (7)$$

where $\langle\ \rangle_{\mathrm{orient}}$ stands for the orientational average.

B. The lattice factor $Z(q)$ for the simple-cubic (sc) lattice

The lattice factor $Z(\mathbf{q})$ for the sc lattice can be calculated by the method of Yarusso *et al.*[22] Their method is to calculate the diffraction pattern from the assembly of randomly oriented paracrystals by taking a rotational average of one infinitely large paracrystal.

Three unit vectors, $\mathbf{a}_1,\mathbf{a}_2,\mathbf{a}_3$, for the ideal sc lattice are taken as shown in Fig. 1(a), and the length is represented by a:

$$|\mathbf{a}_1|=|\mathbf{a}_2|=|\mathbf{a}_3|=a . \quad (8)$$

Then,

$$\mathbf{a}_1\cdot\mathbf{q}=-aq\sin\theta\cos\phi , \quad (9)$$

$$\mathbf{a}_2\cdot\mathbf{q}=aq\sin\theta\sin\phi , \quad (10)$$

$$\mathbf{a}_3\cdot\mathbf{q}=aq\cos\theta . \quad (11)$$

Figure 2 shows the Eulerian angles (θ,η,ϕ) specifying the orientation of the coordinates $(\hat{\mathbf{u}},\hat{\mathbf{v}},\hat{\mathbf{w}})$ fixed to the unit cell with respect to the laboratory fixed coordinate $(\hat{\mathbf{x}},\hat{\mathbf{y}},\hat{\mathbf{z}})$. The $\hat{\mathbf{z}}$ axis is parallel to the vector $\mathbf{q}$, θ and η are the polar and azimuthal angles specifying the orientation of the axis $\hat{\mathbf{w}}$, and ϕ is the angle specifying rotation of the crystal around the $\hat{\mathbf{w}}$ axis. In the case of the sc lattice the axis $\hat{\mathbf{w}}$ coincides with the vector $\mathbf{a}_3$. By assuming the isotropic distortions of a real lattice point from an ideal lattice point designated by $\mathbf{a}_1$, $\mathbf{a}_2$, and $\mathbf{a}_3$ [Fig. 1(a)]

$$\Delta a_1=\Delta a_2=\Delta a_3=\Delta a . \quad (12)$$

We obtain from Eqs. (4)–(6) and (12),

$$Z_1(q,\theta,\phi)=[1-\exp(-q^2\Delta a^2)]/[1-2\exp(-\tfrac{1}{2}q^2\Delta a^2)\cos(-qa\sin\theta\cos\phi)+\exp(-q^2\Delta a^2)] , \quad (13)$$

$$Z_2(q,\theta,\phi)=[1-\exp(-q^2\Delta a^2)]/[1-2\exp(-\tfrac{1}{2}q^2\Delta a^2)\cos(qa\sin\theta\sin\phi)+\exp(-q^2\Delta a^2)] , \quad (14)$$

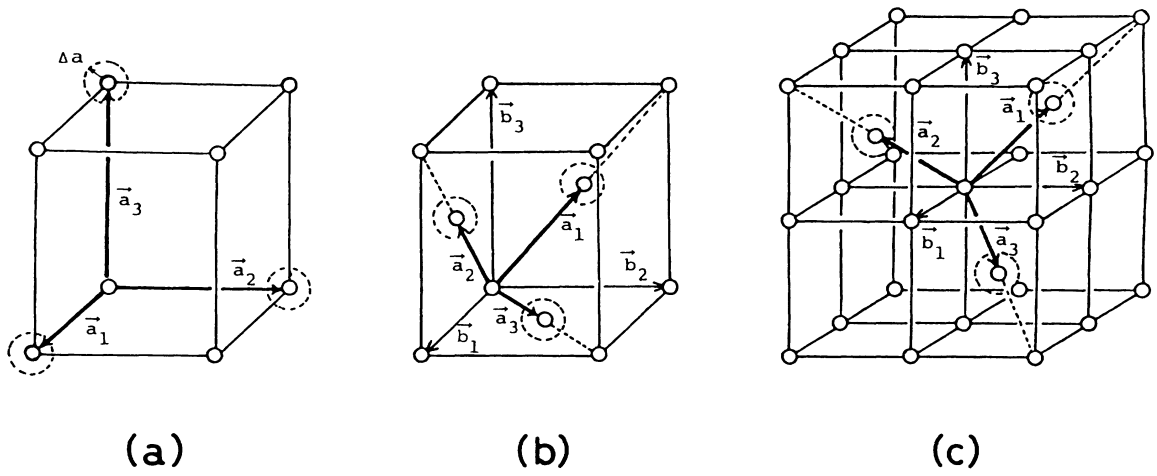

FIG. 1 (a) Three fundamental vectors $\mathbf{a}_1$, $\mathbf{a}_2$, and $\mathbf{a}_3$ for a simple-cubic (sc) lattice. In (a), (b), and (c) the isotropic lattice distortion is depicted by the spheres of radius Δa (dashed circles). (b) The fundamental vectors $\mathbf{a}_1$, $\mathbf{a}_2$, $\mathbf{a}_3$ and the orthogonal vectors $\mathbf{b}_1$, $\mathbf{b}_2$, $\mathbf{b}_3$ for a face-centered-cubic (fcc) lattice. (c) The fundamental vectors $\mathbf{a}_1$, $\mathbf{a}_2$, $\mathbf{a}_3$ and the orthogonal vectors $\mathbf{b}_1$, $\mathbf{b}_2$, $\mathbf{b}_3$ for a body-centered-cubic (bcc) lattice.

$$Z_3(q,\theta,\phi)=[1-\exp(-q^2\Delta a^2)]/[1-2\exp(-\tfrac{1}{2}q^2\Delta a^2)\cos(qa\cos\theta)+\exp(-q^2\Delta a^2)]\ . \tag{15}$$

Then we can calculate $Z(q)$ for the randomly oriented paracrystals by

$$Z(q)=\frac{2}{\pi}\int_0^{\pi/2}\int_0^{\pi/2} Z_1(q,\theta,\phi)Z_2(q,\theta,\phi)Z_3(q,\theta,\phi)\sin\theta\, d\theta\, d\phi\ . \tag{16}$$

C. $Z(q)$ for the face-centered-cubic (fcc) lattice

We define the fundamental vectors $\mathbf{a}_1$, $\mathbf{a}_2$, $\mathbf{a}_3$ and the orthogonal vectors $\mathbf{b}_1$, $\mathbf{b}_2$, $\mathbf{b}_3$ as in Fig. 1(b) and take the $\hat{\mathbf{w}}$ axis parallel to $\mathbf{b}_3$. We obtain

$$\mathbf{a}_1=\tfrac{1}{2}(\mathbf{b}_2+\mathbf{b}_3)\ , \tag{17}$$

$$\mathbf{a}_2=\tfrac{1}{2}(\mathbf{b}_1+\mathbf{b}_3)\ , \tag{18}$$

$$\mathbf{a}_3=\tfrac{1}{2}(\mathbf{b}_1+\mathbf{b}_2)\ . \tag{19}$$

Therefore, using the relations of Eqs. (9)–(11), and noting that $|\mathbf{b}_1|=|\mathbf{b}_2|=|\mathbf{b}_3|=a$, we obtain

$$\mathbf{q}\cdot\mathbf{a}_1=\tfrac{1}{2}qa(\sin\theta\sin\phi+\cos\theta)\ , \tag{20}$$

$$\mathbf{q}\cdot\mathbf{a}_2=\tfrac{1}{2}qa(-\sin\theta\cos\phi+\cos\theta)\ , \tag{21}$$

$$\mathbf{q}\cdot\mathbf{a}_3=\tfrac{1}{2}qa(-\sin\theta\cos\phi+\sin\theta\sin\phi)\ . \tag{22}$$

Then, by assuming Eq. (12) again for the distortion of the lattice points from the ideal lattice designated by $\mathbf{a}_1$, $\mathbf{a}_2$, $\mathbf{a}_3$ in Fig. 1(b) and by using Eqs. (4)–(6) and (20)–(22), we obtain

$$Z_1(q,\theta,\phi)=[1-\exp(-q^2\Delta a^2)]/\{1-2\exp(-\tfrac{1}{2}q^2\Delta a^2)\cos[\tfrac{1}{2}qa(+\sin\theta\sin\phi+\cos\theta)]+\exp(-q^2\Delta a^2)\}\ , \tag{23}$$

$$Z_2(q,\theta,\phi)=[1-\exp(-q^2\Delta a^2)]/\{1-2\exp(-\tfrac{1}{2}q^2\Delta a^2)\cos[\tfrac{1}{2}qa(-\sin\theta\cos\phi+\cos\theta)]+\exp(-q^2\Delta a^2)\}\ , \tag{24}$$

$$Z_3(q,\theta,\phi)=[1-\exp(-q^2\Delta a^2)]/\{1-2\exp(-\tfrac{1}{2}q^2\Delta a^2)\cos[\tfrac{1}{2}qa(-\sin\theta\cos\phi+\sin\theta\sin\phi)]+\exp(-q^2\Delta a^2)\}\ . \tag{25}$$

By substituting Eqs. (23)–(25) into Eq. (16), $Z(q)$ for a randomly oriented fcc lattice can be calculated.

D. $Z(q)$ for the body-centered-cubic (bcc) lattice

The three fundamental vectors $\mathbf{a}_1$, $\mathbf{a}_2$, and $\mathbf{a}_3$, and the orthogonal vectors $\mathbf{b}_1$, $\mathbf{b}_2$, and $\mathbf{b}_3$ are defined as shown in Fig. 1(c). Then,

$$\mathbf{a}_1=\tfrac{1}{2}(-\mathbf{b}_1+\mathbf{b}_2+\mathbf{b}_3)\ , \tag{26}$$

$$\mathbf{a}_2=\tfrac{1}{2}(\mathbf{b}_1-\mathbf{b}_2+\mathbf{b}_3)\ , \tag{27}$$

$$\mathbf{a}_3=\tfrac{1}{2}(\mathbf{b}_1+\mathbf{b}_2-\mathbf{b}_3)\ . \tag{28}$$

By taking the $\hat{\mathbf{w}}$ axis parallel to $\mathbf{b}_3$; noting that $|\mathbf{b}_1| = |\mathbf{b}_2| = |\mathbf{b}_3| = a$; assuming isotropic lattice distortions as given by Eq. (12) from the perfect lattice defined by the vectors $\mathbf{a}_1$, $\mathbf{a}_2$, and $\mathbf{a}_3$ in Fig. 1(c); and by using Eqs. (4)–(6) and (26)–(28), we obtain

$$Z_1(q,\theta,\phi)=[1-\exp(-q^2\Delta a^2)]/\{1-2\exp(-\tfrac{1}{2}q^2\Delta a^2)\cos[\tfrac{1}{2}qa(\sin\theta\cos\phi+\sin\theta\sin\phi+\cos\theta)]+\exp(-q^2\Delta a^2)\}\ , \quad (29)$$

$$Z_2(q,\theta,\phi)=[1-\exp(-q^2\Delta a^2)]/\{1-2\exp(-\tfrac{1}{2}q^2\Delta a^2)\cos[\tfrac{1}{2}qa(-\sin\theta\cos\phi-\sin\theta\sin\phi+\cos\theta)]+\exp(-q^2\Delta a^2)\}\ , \quad (30)$$

$$Z_3(q,\theta,\phi)=[1-\exp(-q^2\Delta a^2)]/\{1-2\exp(-\tfrac{1}{2}q^2\Delta a^2)\cos[\tfrac{1}{2}qa(-\sin\theta\cos\phi+\sin\theta\sin\phi-\cos\theta)]+\exp(-q^2\Delta a^2)\}\ . \quad (31)$$

$Z(q)$ for a randomly oriented bcc lattice can be calculated using Eqs. (16) and (29)–(31).

III. RESULTS OF NUMERICAL CALCULATIONS

We first define the paracrystalline distortion factor g as

$$g \equiv \Delta a/|\mathbf{a}_1| = \Delta a/|\mathbf{a}_2| = \Delta a/|\mathbf{a}_3|\ , \quad (32)$$

where $\mathbf{a}_1$, $\mathbf{a}_2$, and $\mathbf{a}_3$ are the three fundamental vectors as shown in Fig. 1 for sc, fcc, and bcc lattices, and Δa is the distortion of the lattice point from the ideal lattice point as schematically drawn in Fig. 1 with the spheres of radius Δa.

Figure 3 shows the results of numerical calculations of $Z(q)$ for a randomly oriented sc lattice for various g values. At small g values (low degrees of distortion), many sharp peaks appear at the reduced scattering vectors $aq/(2\pi)=(h^2+k^2+l^2)^{1/2}$ characteristic for the sc lattice: the relative peak positions of the first- and higher-order peaks are at 1, $\sqrt{2}$, $\sqrt{3}$, $\sqrt{4}$, $\sqrt{5}$, . . . , and these peaks correspond to diffractions from (100), (110), (111), (200), (210), and so on. As the g value increases, the peaks become lower and broader, and the higher-order peaks disappear. According to Hosemann's prediction for the one-dimensional paracrystal lattice, the nth peak disappears at the g value which satisfies the criterion $gn=0.35$.[1] The corresponding criteria for the sc and bcc lattices will be discussed in Sec. V A.

Figures 4 and 5 show the $Z(q)$ for randomly oriented fcc and bcc lattices, respectively. The relative peak positions of the first- and higher-order diffractions from (111), (200), (220), (311), and (222) planes and so on for the fcc lattice are at 1, $(\frac{4}{3})^{1/2}$, $(\frac{8}{3})^{1/2}$, $(\frac{11}{3})^{1/2}$, $(4)^{1/2}$, etc., respectively. The relative peak positions from (110), (200), (211), (220), and (310) planes and so on for the bcc lattice are at 1, $\sqrt{2}$, $\sqrt{3}$, $\sqrt{4}$, $\sqrt{5}$, etc., respectively. As the g value increases, the peaks become lower and broader for these two cases also. The criterion for the (hkl) diffraction peaks to be resolvable will be discussed also in Sec. V A.

It should be noted that strong zeroth-order scattering exists for the three-dimensional paracrystal, and is especially marked for the sc and bcc lattices. This peculiar effect, which exists even for paracrystals with an infinite size, does not exist for the one-dimensional paracrystal. Further details will be discussed in Sec. V B.

IV. CONSIDERATION OF OTHER DISTORTIONS

A. Thermal oscillation (distortion of the first kind) and the effect of interfacial thickness

The thermal vibration of the particles around the lattice points is one of the paracrystalline distortions called a distortion of the first kind, and the effect of an interfacial diffuse boundary is a problem associated with the variation of the scattering contrast between the particles and the medium at the interface. The two problems are inherent to the particle scattering function, and hence these two effects can be treated mathematically in a similar

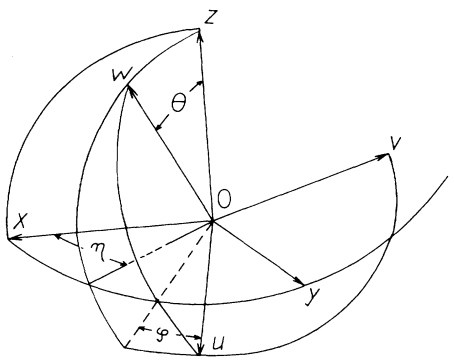

FIG. 2. Eulerian angles (θ,η,ϕ) specifying the orientation of the coordinates $(\hat{\mathbf{u}},\hat{\mathbf{v}},\hat{\mathbf{w}})$ fixed to the unit cell with respect to the laboratory fixed coordinates $(\hat{\mathbf{x}},\hat{\mathbf{y}},\hat{\mathbf{z}})$.

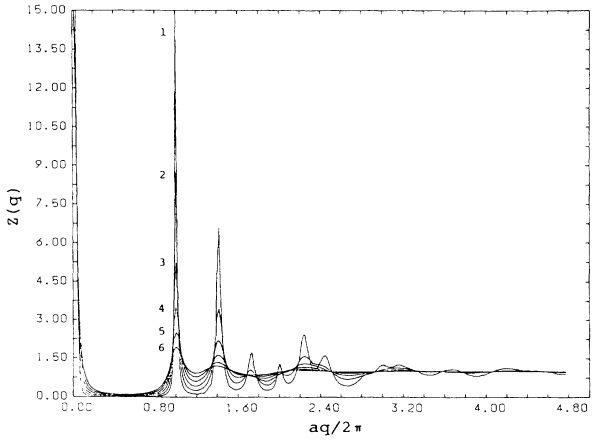

FIG. 3. Calculated paracrystalline lattice factors for a sc structure. $g=0.05$ (curve 1), 0.07 (curve 2), 0.09 (curve 3), 0.11 (curve 4), 0.13 (curve 5), 0.15 (curve 6).

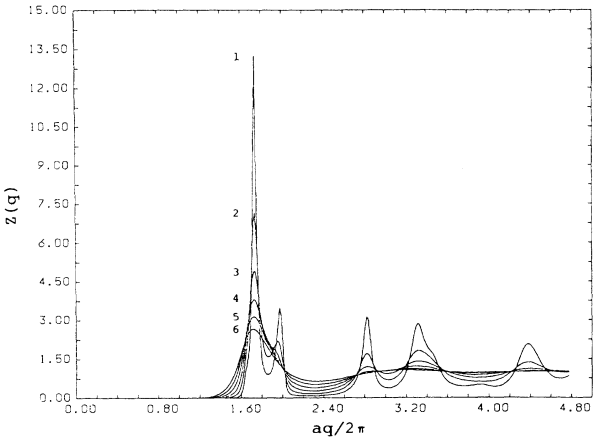

FIG. 4. Calculated paracrystalline lattice factors for a fcc lattice. $g=0.05$ (curve 1), 0.07 (curve 2), 0.09 (curve 3), 0.11 (curve 4), 0.13 (curve 5), 0.15 (curve 6).

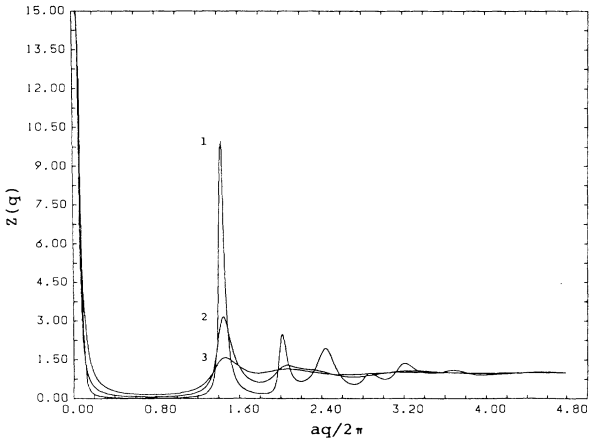

FIG. 5. Calculated paracrystalline lattice factors for a bcc structure. $g=0.05$ (curve 1), 0.09 (curve 2), 0.13 (curve 3).

way. The former effect is given by the exponential term, the so-called Debye-Waller factor, in Eq. (1) as follows:

$$D=\exp(-\tfrac{1}{2}\overline{u^2}q^2)\ , \tag{33}$$

where $\overline{u^2}$ is the mean-square displacement of the particles from the lattice points by thermal motion. Similarly, the effect of the smooth diffuse boundary is given by[23]

$$B=\exp(-\tfrac{1}{2}\sigma_s^2 q^2)\ , \tag{34}$$

where B is the Fourier transform of the smoothing function $b(\mathbf{r})$ characterizing the distribution of the scattering contrast $\rho(\mathbf{r})$ at the interface

$$\rho(\mathbf{r})=\rho_i(\mathbf{r})\circ b(\mathbf{r})\ , \tag{35}$$

where $\rho_i(\mathbf{r})$ is the scattering contrast profile for the sharp interface with $\sigma_s=0$ and

$$b(\mathbf{r})=(2\pi\sigma_s^2)^{-3/2}\exp(-r^2/2\sigma_s^2)\ . \tag{36}$$

For the particles with the diffuse boundary, f_0 in Eq. (1) should be replaced by $f_0B(q)$. Physically, these two effects can be recognized as the blur of the particle scattering. (See Ref. 15 and Fig. 10 in Ref. 24 as examples of the influence of these factors on scattering behavior.) It must be noted that these effects influence the intensity of diffraction peak(s) and even more strongly those of the higher-order peaks. However, the influence on the width of the peaks is very small as is easily seen from Eqs. (1), (33), and (34).

B. Effect of size of the paracrystals

The size of the crystal also affects the scattering behavior. The smaller the crystal, the lower the intensity of the diffraction and the broader the diffraction profile. Therefore, the scattering function $I(q)$ must be calculated taking into consideration the effect of the finite crystal size especially for an assembly of microparacrystals, and even more so for greatly distorted microparacrystals because it is hardly feasible that a greatly distorted crystal can grow into a larger crystal. For an assembly of the microcrystals, the definition of the crystal size is rather obvious. For greatly distorted continuous crystals, however, the situation is not simple. The "crystal size" implies now the limit of "correlation" of lattice points; if the crystal size is N by particle number in one direction, the lattice point of the $(N+1)$th particle is not affected by that of the particle at the origin. Generally, the correlation is a statistical quantity and N is an ensemble-averaged quantity.

The effect of the finite size of the paracrystal is incorporated in Eq. (1) by the shape factor $\Sigma(\mathbf{q})^2$. However, from the technical point of view in the numerical calculation, it seems to be much easier to calculate directly the scattering of the paracrystal containing N particles in each direction specified by the fundamental vectors $\mathbf{a}_1$, $\mathbf{a}_2$, $\mathbf{a}_3$, rather than taking a convolution of the lattice factor Z for infinitely large paracrystals and Σ^2 as in Eq. (1).

One of us (T.H.) previously presented full details of the equation for the lattice factor Z containing N unit cells for the one-dimensional paracrystal,[25] the results of which can be extended to the three-dimensional paracrystals. With this approach instead of Eqs. (1) and (4), we obtain

$$I(\mathbf{q})=N(\langle|f_0|^2\rangle-|\langle f_0\rangle|^2)+N|\langle f_0\rangle|^2[1-D^2(\mathbf{q})] + |\langle f_0\rangle|^2\prod_{k=1}^{3}N_k(Z_k+I_{ck}/N_k)\ , \tag{37}$$

where $N=N_1N_2N_3$ is the total number of unit cells in the paracrystal, N_k the number of the unit cell along the kth direction, Z_k the lattice factor for infinitely large paracrystals along the kth direction, and I_{ck} the zeroth-order scattering related to the finite-size effect of the paracrystal. The factor Z_k is given by Eq. (4b), and I_{ck} is given by

$$I_{ck} = -2\,\mathrm{Re}[F_k(1-F_k^{N_k})/(1-F_k)^2] \tag{38a}$$

$$= -2\,|F_k|\{(1+|F_k|^2)\cos(\mathbf{q}\cdot\mathbf{a}_k) - 2|F_k| - |F_k|^{N_k}\cos[(N_k+1)\mathbf{q}\cdot\mathbf{a}_k] + 2|F_k|^{N_k+1}\cos[N_k(\mathbf{q}\cdot\mathbf{a}_k)] - |F_k|^{N_k+2}\cos[(N_k-1)\mathbf{q}\cdot\mathbf{a}_k]\}/[1-2|F_k|\cos(\mathbf{q}\cdot\mathbf{a}_k)+|F_k|^2]^2 . \tag{38b}$$

Again the assumptions of the independent distance statistics in each direction and between the three directions were employed in the calculation. The intensity $I(q)$ is subjected to the orientational average as in Eq. (7) when the paracrystals have an orientation distribution with respect to the laboratory coordinate. For example, $Z(q,N_c)$ is defined as a lattice factor per unit size, i.e., normalized by $N_1N_2N_3 \equiv N_c^3$ for the randomly oriented paracrystal with $N_1 = N_2 = N_3 \equiv N_c$:

$$Z(q,N_c) = \left\langle \prod_{k=1}^{3} [Z_k + (I_{ck}/N_k)] \right\rangle_{\text{random orient}} . \tag{39}$$

Figure 6 shows results of the numerical calculations of $Z(q,N_c)$ for three different N_c values and at a fixed g value for the fcc lattice. The intensity level of each profile was shifted vertically to avoid overlapping. It obviously approaches unity at large q, regardless of the value of N_c. With decreasing N_c, the diffraction peak(s) clearly become lower and broader, and the higher-order peaks tend to be smeared. The upturn of a scattering curve at low-angle regions, which is observed for a small value of N_c, corresponds to the contribution of the zeroth-order scattering I_{ck} from the finite size of the paracrystal. In this calculation, the volume outside the paracrystal is assumed to be a vacuum; therefore, this upturn appears. If the difference in the electron densities or the scattering length inside and outside of the paracrystal is zero, this upturn would disappear.

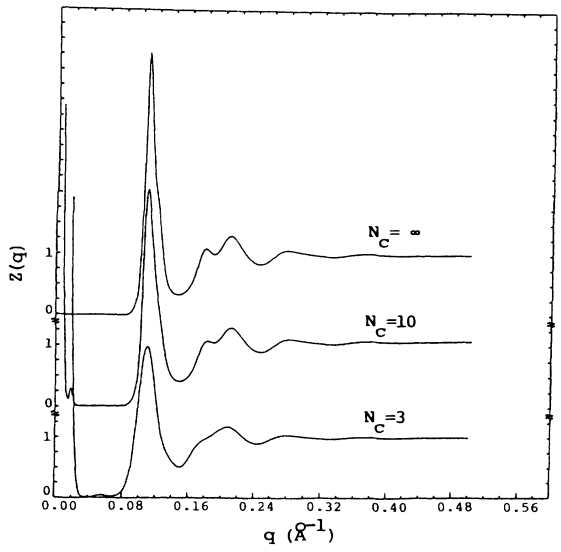

FIG. 6. Effects of the crystal size on the paracrystalline lattice factor for fcc with the nearest-neighbor distance $a_n = 70.7$ Å. Each curve was vertically shifted to avoid an overlap. g was 0.10.

As both of the parameters g and N simultaneously affect the height and the width of the diffraction peak, it is fairly difficult to determine unique values of g and N from a single diffraction maximum.[26] Hosemann and his coworkers found experimentally that the values of g and N should not be independent. They proposed the so-called α^* law,[27]

$$g\sqrt{N} = \alpha^* , \quad 0.1 < \alpha^* < 0.2 . \tag{40}$$

This α^* law may be used for the approximate determination of g and N. It is a very interesting problem to examine whether the α^* law holds in such systems as latex dispersion and block copolymers which have not been tested so far.

V. DISCUSSIONS ON CRITERION FOR THE (*hkl*) DIFFRACTION MAXIMUM TO BE RESOLVED AND ON $Z(q \to 0)$ FOR THE THREE-DIMENSIONAL PARACRYSTALS

A. Criterion for the (*hkl*) diffraction maximum to be resolved for the three-dimensional paracrystals

Hosemann predicted the following equation as the criterion for the nth peak to be resolved for the one-dimensional paracrystal:

$$gn = 0.35 . \tag{41}$$

This relation was obtained analytically on the assumption that the relation

$$Z_{\max}/Z_{\min} = 1.5 \tag{42}$$

was a limit for the nth peak to be resolved, where $Z_{\max}$ was a value of $Z(q)$ at the nth peak position and $Z_{\min}$ was a corresponding minimum value.

We reexamined this relation in our numerical calculations for a one-dimensional paracrystal. Figure 7 shows the g_l-versus-n^{-1} plot for a one-dimensional paracrystal, where g_l is the value g which satisfies Eq. (42). The straight line is the result of the first-order least-squares fitting of the data points, which predicts the following relation:

$$g_l n = 0.319 . \tag{43}$$

The slight discrepancy between Eqs. (41) and (43) may be due to the approximations involved in the procedure of obtaining Eq. (41) analytically.

For three-dimensional paracrystals, the situation becomes much more complicated, because each scattering

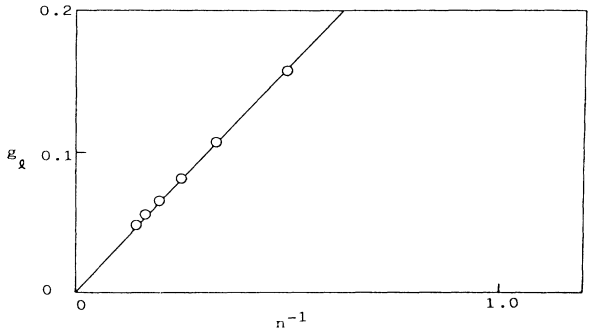

FIG. 7. g_l-vs-n^{-1} plot for a one-dimensional paracrystal. The straight line is a result of the first-order least-squares fitting, $g_l=0.319n^{-1}$.

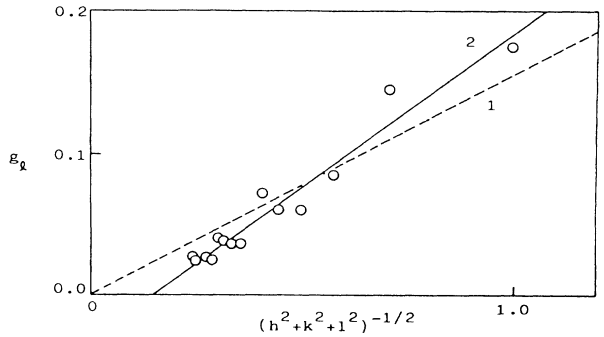

FIG. 8. g_l-vs-$(h^2+k^2+l^2)^{-1/2}$ plot for a sc lattice. The straight lines are the results of the first-order least-square fitting. Line 1, $g_l=0.155\times(h^2+k^2+l^2)^{-1/2}$; line 2, $g_l=0.215\times(h^2+k^2+l^2)^{-1/2}-0.0313$.

peak corresponds not only to a different order but also to a different reflection plane which has different multiplicity. Furthermore, the extinction rule has to be taken into account. Thus it seems to be impossible to obtain analytically a criterion for the three-dimensional paracrystal. Therefore we tried to obtain the criterion by the numerical calculations of the lattice factor with an infinite size.

Figure 8 shows the g_l-versus-$(h^2+k^2+l^2)^{-1/2}$ plot for a simple-cubic paracrystal. It is obvious that the linearity is not as good as for the case of the one-dimensional paracrystal, as we expected. The straight lines are obtained by the first-order least-squares fitting by two functions, $y=ax$ and $y=ax+b$. These fittings give us the following relations:

$$g_l(h^2+k^2+l^2)^{1/2}=0.155\ , \tag{44}$$

$$g_l=0.215(h^2+k^2+l^2)^{-1/2}-0.031\ , \tag{45}$$

which may be used as criteria for the simple-cubic paracrystal lattice. As is clearly seen from Fig. 8, Eq. (45) gives a better fit. However, this equation predicts that the higher-order peaks, whose $(h^2+k^2+l^2)$ values are larger than 48, cannot appear even if the g value is zero (i.e., for the ideal crystal). This is physically unreasonable. Actually, in the three-dimensional paracrystal the relation between g_l and $(h^2+k^2+l^2)$ may not be a simple linear relation. Hence Eq. (45) is an approximate criterion. The value specifying the criterion for the three-dimensional paracrystal appears to be close to that for the one-dimensional paracrystal divided by $\sqrt{3}$ (viz. $0.35/\sqrt{3}=0.202$).

For the bcc lattice, the following approximate criteria were obtained using reflections from (110), (200), (211), (220), (310), and (321) planes:

$$g_l(h^2+k^2+l^2)^{1/2}=0.170\ , \tag{46}$$

$$g_l=0.215(h^2+k^2+l^2)^{-1/2}-0.024\ . \tag{47}$$

As was the case for the sc lattice, Eq. (47) is a better criterion. It is interesting to note that we obtain similar criteria for sc and bcc lattices. It was impossible to obtain a criterion for the fcc lattice because the fusion of the peaks hindered the estimation of the characteristic $Z_{\max}$ and $Z_{\min}$ values for each peak.

B. Behavior of the lattice factor Z at $q\to 0$ for the cubic paracrystals

In this section we discuss the origin of the intensity upturn for Z in the limit of $q\to 0$ which was found clearly for sc (Fig. 3) and bcc (Fig. 5) lattices. This intensity upturn may be thought peculiar in light of the behavior of Z for the one-dimensional paracrystal as reported by Hosemann and Wilke.[28] For the one-dimensional paracrystal it was found that

$$\lim_{q\to 0} Z(q)=g^2\ . \tag{48}$$

As q approaches zero, the intensity $Z(q)$ continuously decreases to the limiting value of g^2 and the intensity upturn is not found.

For a three-dimensional paracrystal, we should study Eq. (4) to understand this upturn. For example, $Z_3(\mathbf{q})$ can be calculated as follows:

$$1-|F_3|^2=q^2\Delta a_3^2+O(q^4)\ , \tag{49}$$

$$1-2|F_3|\cos(\mathbf{q}\cdot\mathbf{a}_3)+|F_3|^2=[4\sin^2(\tfrac{1}{2}a_3q\cos\theta)](1-\tfrac{1}{2}q^2\Delta a_3^2)+O(q^4)$$
$$=a_3^2q^2\cos^2\theta+O(q^4)\ . \tag{50}$$

Thus it follows that

$$\lim_{q\to 0} Z_3(q)=\frac{\Delta a_3^2}{a_3^2\cos^2\theta}\equiv\frac{\Delta a_3^2}{a_{3,\text{eff}}^2}\equiv g_{3,\text{eff}}^2 \tag{51}$$

for a one-dimensional paracrystal with periodicity along the a_3 direction and observation of the scattering with $\mathbf{q}$ vector along the $\mathbf{a}_3$ direction, $\cos\theta=1$, and hence

$$\lim_{q\to 0} Z_3=\Delta a_3^2/a_3^2=g_3^2\ , \tag{52}$$

which was obtained by Hosemann and Wilke. However, for three-dimensional crystals, the effective unit-cell size $a_{3,\text{eff}}\equiv a_3\cos\theta$, which is a projection of $\mathbf{a}_3$ onto $\mathbf{q}$, depends on the orientation of the vector $\mathbf{a}_3$ with respect to $\mathbf{q}$. Thus the limiting value of Z at $q\to 0$ is equal to the effective g value (g_{eff}) as defined in Eq. (51), which goes to infinity as θ approaches $\pi/2$. This divergence, which causes the upturn of $Z(q)$ as q goes to zero, occurs as a consequence of a random orientation of the paracrystal and of a spherically symmetric distortion of the lattice points, e.g., $\Delta a_{31}=\Delta a_{32}=\Delta a_{33}\equiv\Delta a_3$. Similar to Eq. (51), we obtain

$$\lim_{q\to 0} Z_1(q)=\frac{\Delta a_1^2}{a_1^2\sin^2\theta\cos^2\phi}\equiv\frac{\Delta a_1^2}{a_{1,\text{eff}}^2}\equiv g_{1,\text{eff}}^2\ , \tag{53}$$

$$\lim_{q\to 0} Z_2(q)=\frac{\Delta a_2^2}{a_2^2\sin^2\theta\sin^2\phi}\equiv\frac{\Delta a_2^2}{a_{2,\text{eff}}^2}\equiv g_{2,\text{eff}}^2\ . \tag{54}$$

Therefore

$$\lim_{q\to 0} Z(q)=\prod_{k=1}^{3} g_{k,\text{eff}}^2\ . \tag{55}$$

We may extend similar arguments for fcc and bcc.

VI. COMPARISON WITH EXPERIMENTAL SCATTERING PROFILES

In recent years scattering techniques have been employed for the investigation of the ordering phenomena[5-7] of macroions (including synthetic macroions,[29] biopolymers,[24] and ionic surfactant micelles[30]) in solutions. Laser light and neutron scattering techniques have also been used for solutions of monodisperse polymer latex particles.[31-33] The ordering of larger latex particles with a diameter of about 3000 Å in solution has been almost unequivocally proven by observation through ultramicroscopy.[9] SAXS and SANS techniques have been used to study the microdomain structure of block copolymers in the solid state[15-17] and in solutions.[18,19] In this section we discuss the applications of the three-dimensional paracrystal theory to some real systems, ordered spherical microdomains of block polymers and aqueous suspensions of ordered latex particles.

A. Small-angle x-ray scattering of block copolymers

As a model experimental system showing ordered spherical microdomains with a cubic symmetry, we discuss here the solvent-cast film of a polystyrene-polyisoprene block polymer designated as SI-4 with a total number-average molecular weight $M_n=21.9\times 10^4$ and a weight percent of polyisoprene block $w_{ps}=15.4$. Readers who are interested in the morphology, physics, and details of the block polymers are referred to the earlier references.[15,18,19,34]

Figure 9 shows the SAXS profile obtained for the solvent-cast films of SI-4 (shown by the points[15]). The profile was corrected for the slit-width and slit-height

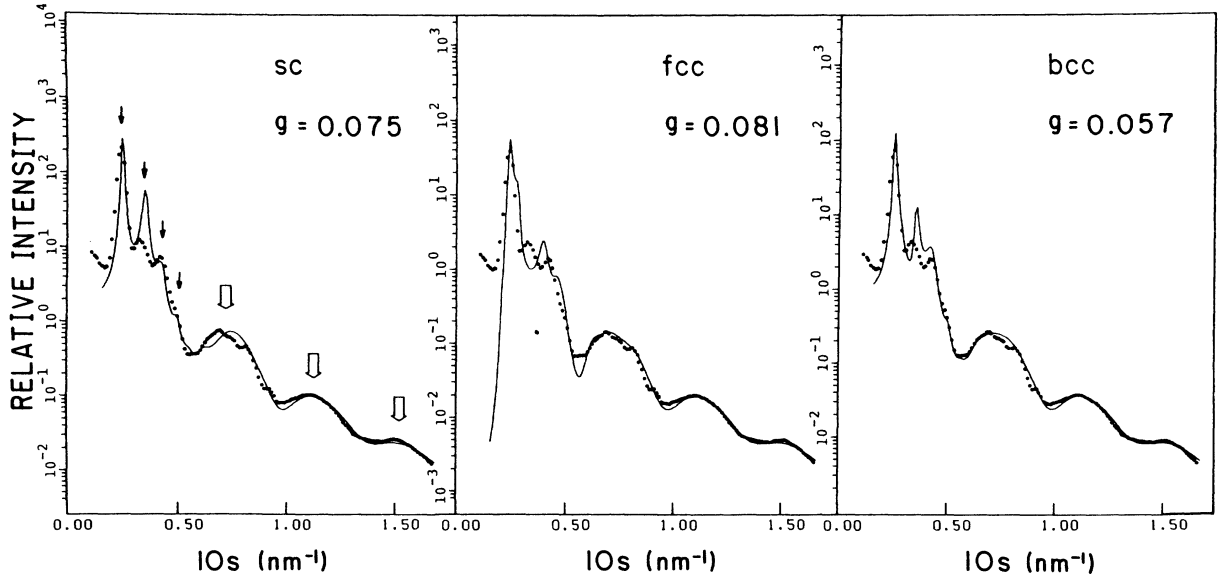

FIG. 9. Comparison of the experimental scattering curve of styrene-isoprene block copolymer and the theoretical curves for cubic paracrystals: (a) sc, (b) fcc, and (c) bcc. Theoretical profiles were calculated for a given set of parameters $R=12.9$ nm, $\sigma_r=1.0$ nm, and $\sigma_s=0.5$ nm. The parameters g and a_n were 0.075 and 40.1 nm, respectively, for sc, 0.081 and 69.6 for fcc, and 0.057 and 56.7 for bcc.

smearing and for the background scattering due to diffuse thermal scattering. The figure also includes the best-fit theoretical profiles with an infinitely large size (the profiles drawn in the solid curves). In these three figures the experimental profiles are the same and s denotes $s=q/2\pi$.

In the experimental profile the scattering maxima marked by thin arrows are due to those from interparticle interference associated with $Z(q,N_c)$ or $Z(q)$, their relative positions being $1:\sqrt{2}:\sqrt{3}:\sqrt{4}$. The maxima marked by thick arrows are due to those from higher-order scattering maxima from intraparticle interference. In these higher-angle regions $Z(q,N_c)$ or $Z(q)$ approaches unity, so that the scattering depends upon the single-particle scattering $|\langle f_0\rangle|^2$. The small modulation on the first-order scattering maximum due to the intraparticle interference located at $s\approx 0.70\times 10^{-1}$ nm^{-1} may be associated with the interparticle interference phenomena [i.e., the higher-order maxima occurring in $Z(q)$].

To obtain the best-fit theoretical curve we need structure parameters such as (i) the average radius of the spherical domain R and (ii) its standard deviation σ_r, (iii) the parameter characterizing the diffuse boundary σ_s, (iv) the length $a_n=|\mathbf{a}_1|=|\mathbf{a}_2|=|\mathbf{a}_3|$ for the fundamental lattice vectors, identical to the nearest-neighbor distance between the particles and (v) the paracrystalline distortion parameter $g\equiv\Delta a/a_n$ which is assumed to be isotropic, and (vi) the lattice symmetry (sc, fcc, or bcc). Among these, the parameters R, σ_r, and σ_s were obtained previously from the higher-angle region where $Z(q)\rightarrow 1$ and are commonly used for the three figures for the best fitting.[15] The theoretical and experimental profiles of the sc, fcc, and bcc lattices indicate that the bcc lattice of $a_n=567$ Å and $g=0.057$ is the most probable one. The slight misfit may be attributed to the distortion of the real lattice from the cubic lattice which in turn may arise from the residual strain imposed on the film during solvent evaporation. Further investigations along this line should be done for the block polymer solutions at a given temperature and concentration.

It is worth noting that, as expected, the value $g=0.057$ is very small compared with the values for colloidal suspensions to be discussed in the next section, and is of about the same level as for the lamellar microdomains of the block polymers.[35] From the g value we can determine the heterogeneity index $\mathcal{I}_{an}$ for the distribution of the nearest-neighbor distance.[35] The index $\mathcal{I}_{an}$ is defined as

$$\mathcal{I}_{an}=\langle a_n^2\rangle/\langle a_n\rangle^2=\langle a_n\rangle_w/\langle a_n\rangle_n=g^2+1\ , \tag{56}$$

where a_n is the nearest-neighbor distance, $\langle a_n^2\rangle$ and $\langle a_n\rangle$ the second and the first moments of its distribution function, and $\langle a_n\rangle_w$ and $\langle a_n\rangle_n$ are the weight and number average distances, respectively. The index $\mathcal{I}_{an}=1.003$ is obtained for $g=0.057$, indicating a highly regular arrangement of the domain in the superlattice. Similarly, the heterogeneity index of the size of the spherical domains $\mathcal{I}_R$ can be estimated from σ_r/R by

$$\mathcal{I}_R=(\sigma_r/R)^2+1\ . \tag{57}$$

Since $\sigma_r/R\simeq 0.078$, $\mathcal{I}_R=1.006$. Thus the domain-size distribution itself is also very narrow.

Figure 10 shows the calculated scattering profiles for sc, fcc, and bcc cubic paracrystals with random orientations and infinitely large crystals for several g values: (a) $g=0.05$, (b) $g=0.07$, and (c) $g=0.08$. Other parameters such as R, σ_r, σ_s, and a_n are all fixed for the three figures ($R=129$ Å, $\sigma_r=10$ Å, $\sigma_s=5$ Å, and $a_n=567$ Å). These figures clearly indicate how the scattering profiles depend on the packing and the distortion. The profiles can be used as a chart to estimate quantitatively the packing and the distortion of the real microdomain systems.

B. Small-angle neutron and laser light scattering of polymer latex suspensions

In colloid science, the lattice factor $[Z(q)]$ is often called the interparticle interference function, and represented by $S(q)$. All the $S(q)$ functions which we discuss in this section are obtained from the scattering curve with the assumption of $\sigma_r=\sigma_s=0$, i.e., the latex particles are homogeneous spheres and monodisperse. The scattering intensity in Eq. (3) is rewritten by

$$I(q)=NP(q)S(q)\ , \tag{58}$$

$$P(q)=|f_0|^2,\quad S(q)=Z(q)\ , \tag{59}$$

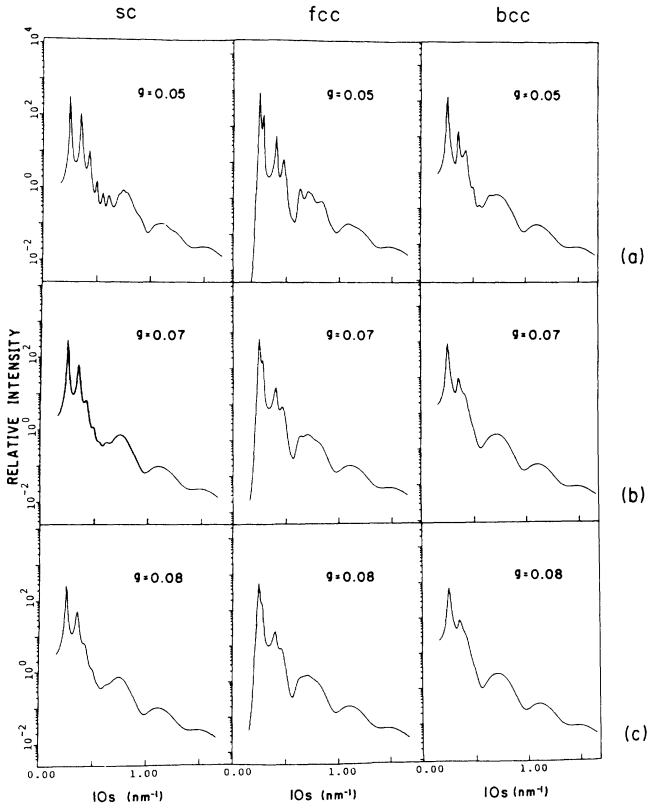

FIG. 10. Theoretical scattering curves of cubic paracrystals. (a) $g=0.05$, (b) $g=0.07$, and (c) $g=0.08$. Other parameters are the same as in Fig. 9.

where $P(q)$ is the intraparticle scattering function. All the interference functions $Z(q)$ are obtained for $N_c \to \infty$ unless otherwise stated.

In Fig. 11 we give the interference function for a polymer latex dispersion obtained by laser light scattering[31] (solid circles) and $Z(q)$ calculated by the present theoretical treatment (solid curve). The concentration of latex particles is much lower than those employed in microscopic observation to avoid some experimental difficulties such as multiple scattering. We cannot observe directly the spatial distribution of the particles by microscopy for this system. However, it is expected that the spatial arrangement of the particles will be highly distorted due to the low concentrations. The first peak position and height were fitted with a g value of 0.19 for fcc, though the observed height of the secondary peak could not be reproduced well by the theory.

In Fig. 12 the interference functions obtained by neutron scattering for latex solutions[32] are compared with the theoretical curves which were obtained for fcc structures. Investigations on the more concentrated dispersions were possible for small latex particles by employing the SANS technique. Here again the first peak position and height were fitted. Although the disagreement at low scattering vectors and for the secondary peak are obvious, the agreement between theory and experiment is satisfactory. The g values are again about 0.2. With decreasing concentration, the g value becomes larger. This trend is quite understandable and is consistent with the microscopic observation.[36] Also, the tendency of the interparticle spacing to decrease with increasing concentration (volume fraction is denoted by ϕ') is readily acceptable and is in accordance with earlier microscopic observations.[37]

Figure 13 shows the experimentally obtained interference function for polymer latex dispersion from light scattering[33] and the theoretical curve obtained for an fcc structure with a g value of 0.15. The agreement is fairly satisfactory, though the agreement for the second peak is not as good. The disagreement in the low-angle regions is also clear, but it may be at least partially due to the inaccuracy in the experimental data caused by multiple scattering, dust scattering, etc.

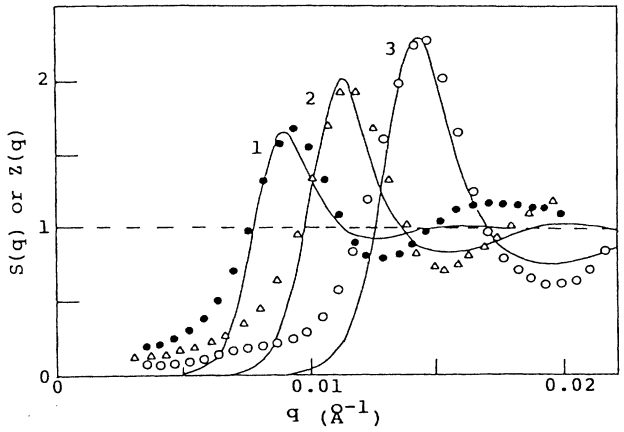

FIG. 12. Comparison of the experimental interference function $S(q)$ obtained by neutron scattering for latex solutions by Cebula *et al.* and theoretical lattice factors, $Z(q)$. ●, △, and ○ represent $S(q)$ observed for a latex of $R = 157$ Å at $\phi' = 0.04$, 0.08, and 0.13, respectively. Curves 1, 2, and 3 represent $Z(q)$ for fcc structures with $a_n = 830$ Å, $g = 0.22$; $a_n = 679$ Å, $g = 0.19$; and $a_n = 539$ Å, $g = 0.17$, respectively.

Figure 14 shows the experimental data given in Fig. 12 for a volume fraction (ϕ') of 0.13, together with theoretical curves, which were obtained for two different sets of N_c and g. The profile for the smaller N_c and g values gives a better fit with the experimental data; although we cannot claim that this pair of g and N_c values ($g = 0.12$, $N_c = 3$) is the only pair which can reproduce this $S(q)$ curve, because both g and N_c simultaneously affect the peak height and the peak width as was discussed in Sec. IV B. It might be interesting to note the rough agreement of these values with the α^* law ($\alpha^* = 0.12 \times 3^{1/2} = 0.207$). As will be discussed in detail later, the interparticle dis-

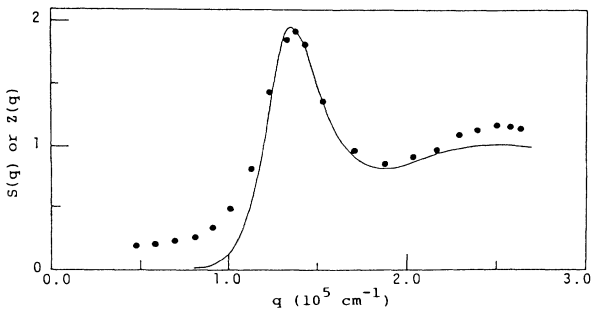

FIG. 11. Comparison of the experimental interference function $S(q)$ with theoretical paracrystalline lattice factor, $Z(q)$. Circles: $S(q)$ for latex solution by Ottewill, volume fraction (ϕ'), 10^{-3}; particle radius, 256 Å. Line: $Z(q)$ for an fcc structure, $a_n = 5597$ Å, $g = 0.19$.

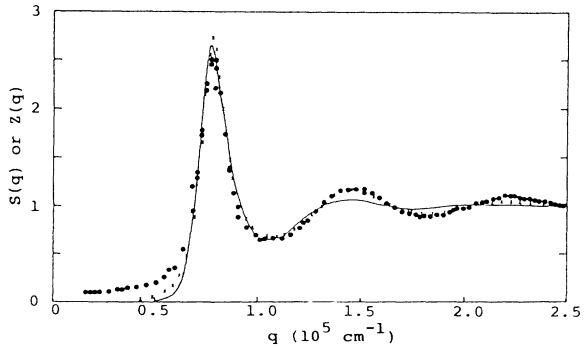

FIG. 13. Comparison of the experimental interference function $S(q)$ and theoretical paracrystalline lattice factor $Z(q)$. Circles: $S(q)$ obtained by light scattering for latex solution by Versmold *et al.*, 1.34×10^{18} particles/m^3. Line: $Z(q)$ for an fcc structure. $a_n = 9824$ Å, $g = 0.15$. ×: RMSA result.

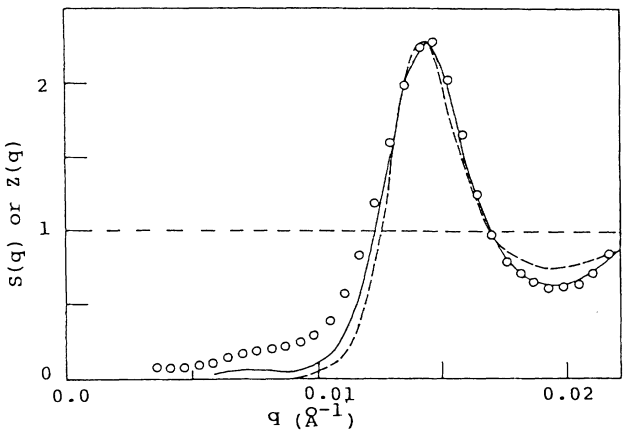

FIG. 14. Comparison of the experimental interference function $S(q)$ and theoretical lattice factors $Z(q)$. Circles: $S(q)$ obtained by neutron scattering for a latex solution (Ottewill *et al.*), $\phi'=0.13$, $R=157$ Å. Dashed curve: $Z(q)$ for an fcc structure, $a_n=539$ Å, $g=0.17$, $N_c=\infty$. Solid curve: $Z(q)$ for an fcc structure. $a_n=539$ Å, $g=0.12$, $N_c=3$.

tance obtained from the $S(q)$ peak position is very close to the one calculated assuming a uniform distribution. Thus, we believe that the crystal size, in this case, must be recognized as the region which has correlated particles for the directions of the three axes as described in Sec. IV B.

Note that the interparticle distances a_n used in the calculation of $Z(q)$ in Figs. 11–14 are all fairly close to the average interparticle spacing ($2D_0$) which can be calculated from the concentration by assuming a uniform distribution of the particles throughout the space and fcc symmetry.[38] In the case of Fig. 11, the a_n value was 5600 Å whereas the $2D_0$ value was 4633 Å for fcc. For Fig. 12 the agreement is even much better: The values of a_n were 830, 679, and 539 Å at the volume fractions of 0.04, 0.08, and 0.13, respectively, whereas the $2D_0$ values were 831, 659, and 561 Å. In Fig. 13 the value a_n was 9824 Å and the $2D_0$ value was 10180 Å. Except for a case in Fig. 11, the two interparticle spacings are fairly close to each other. This agreement and the fact, that the experimental scattering profiles were well reproduced by the theoretical profile for the fcc lattice, support the validity of the present extension of the paracrystal theory.

Another interesting point is the similarity between the interference functions calculated by the so-called rescaled mean spherical approximation (RMSA) method and those calculated by our present treatment. The RMSA results are shown by crosses in Fig. 13, which were taken from the work by Versmold and co-workers.[33] Our values, calculated on the basis of the paracrystalline theory, are in fairly good agreement not only with the observed $S(q)$ but also with the RMSA results. The RMSA method is based on a liquid theory, whereas the paracrystalline theory has its foundation in ideal lattices. Thus the agreement shown by the two methods might indicate that the nature of the ordered structure under consideration is intermediate between a liquid and a solid. The RMSA method is based on a purely repulsive interaction, whereas in our approach the type of the interaction does not explicitly come into question. Thus, it is not warranted to claim that the interparticle interaction is purely repulsive on the basis of the agreement of the RMSA calculation with the observed $S(q)$. In order to clarify the nature of the interparticle interaction, the analysis of the structure factor in terms of the RMSA method is not adequate: a much more thorough study is required of the scattering behavior and of other fundamental physicochemical properties of the systems as well.

VII. CONCLUSION

In the present article a three-dimensional paracrystal theory has been developed for cubic lattices. The lattice factors were calculated by taking the paracrystalline distortion into account. Also discussed were the thermal oscillation of the scattering elements around the lattice point, the interfacial thickness, and the size of the paracrystals. The theory was compared with scattering profiles obtained for block copolymer (solid) films and polymer latex suspensions. From the comparison, the lattice symmetry and the degree of paracrystalline distortion were evaluated. The best fit was obtained for microdomain distribution in the copolymer film, when bcc structures with relatively small distortions were assumed. The fcc structures with fairly large distortions gave the best fit with the latex suspensions studied.

ACKNOWLEDGMENTS

Valuable suggestions were received from Professor G. Hall, to whom our sincere thanks are due. Financial support from the Ministry of Education, Science, and Culture (grant in aids for Specially Promoted Research) are sincerely acknowledged.

*To whom correspondence should be addressed.

[1]R. Hosemann and S. N. Bagchi, *Direct Analysis of Diffraction by Matter* (North-Holland, Amsterdam, 1962).
[2]W. Frank and W. Wilke, Colloid Polym. Sci. **261**, 1010 (1983).
[3]R. Steffen and R. Hosemann, Phys. Rev. B **13**, 3232 (1976).
[4]O. Glatter and O. Kratky, *Small-Angle X-ray Scattering* (Academic, London, 1982), Chap. 4.
[5]N. Ise and T. Okubo, Acc. Chem. Res. **13**, 303 (1980).
[6]N. Ise, Makromol. Chem. **12**, 215 (1985).
[7]N. Ise, Angew, Chem. Int. Ed. Engl. **25**, 323 (1986).
[8]W. Luck, M. Klier, and H. Wesslau, Ber. Bunsenges. Phys. Chem. **67**, 75 (1963).
[9]A. Kose, M. Ozaki, K. Takano, Y. Kobayashi, and S. Hachisu, J. Colloid Interface Sci. **44**, 330 (1973).

[10]N. A. Clark, A. Hard, and B. J. Ackerson, Nature **281**, 57 (1979); Ackerson and N. A. Clark, Phys. Rev. Lett. **46**, 123 (1981).
[11]T. Yoshiyama, I. Sogami, and N. Ise, Phys. Rev. Lett. **53**, 2153 (1984).
[12]R. M. Cornell, J. W. Goodwin, and R. H. Ottewill, J. Colloid Interface Sci. **71**, 254 (1979).
[13]N. Ise, T. Okubo, K. Ito, S. Dosho, and I. Sogami, Langmuir **1**, 176 (1985).
[14]N. Ise, K. Ito, T. Okubo, S. Dosho, and I. Sogami, J. Am. Chem. Soc. **107**, 8074 (1985).
[15]T. Hashimoto, M. Fujimura, and H. Kawai, Macromolecules **13**, 1660 (1980).
[16]F. S. Bates, R. E. Cohen, and C. V. Berney, Macromolecules **15**, 589 (1982).
[17]D. J. Kinning and E. L. Thomas, Macromolecules **17**, 1712 (1984).
[18]M. Shibayama, T. Hashimoto, and H. Kawai, Macromolecules **16**, 16 (1983).
[19]T. Hashimoto, M. Shibayama, H. Kawai, H. Watanabe, and T. Kotaka, Macromolecules **16**, 361 (1983).
[20]Thomas and co-workers (Ref. 17) attempted to compare the experimental profiles with the profiles calculated based upon a Percus-Yevick–type potential function between the spherical domains. However, this approach to the block polymer systems is phenomenological and best applied to the systems with a large distortion so that the higher-order maxima due to the cubic lattice symmetry do not exist.
[21]R. Bramer and W. Ruland, Makromol. Chem. **177**, 3601 (1976).
[22]D. J. Yarusso and S. L. Cooper, Macromolecules **16**, 1871 (1983).
[23]W. Ruland, J. Appl. Crystallogr. **4**, 70 (1971).
[24]H. Matsuoka, N. Ise, T. Okubo, S. Kunugi, H. Tomiyama, and Y. Yoshikawa, J. Chem. Phys. **83**, 378 (1985).
[25]T. Hashimoto, A. Todo, and H. Kawai, Polym. J. **10**, 521 (1978).
[26]It is well known that, if the scattering profile contains more than two diffraction maxima from the lattice, we can separate the effects of g and N by analyzing the peak breadth as a function of the order of the diffractions (Ref. 1).
[27]F. J. Balta-Calleja and R. Hosemann, J. Appl. Crystallogr. **13**, 521 (1980).
[28]R. Hosemann and W. Wilke, Makromol. Chem. **118**, 230 (1968).
[29]N. Ise, T. Okubo, S. Kunugi, H. Matsuoka, K. Yamamoto, and Y. Ishii, J. Chem. Phys. **81**, 3294 (1984).
[30]Y. Ishii, H. Matsuoka, and N. Ise, Ber. Bunsenges. Phys. Chem. **90**, 50 (1986).
[31]R. H. Ottewill, Progr. Colloid Polymer Sci. **67**, 71 (1980).
[32]D. J. Cebula, J. W. Goodwin, G. C. Jeffrey, R. H. Ottewill, A. Parentich, and R. A. Richardson, Faraday Discuss. Chem. Soc. **76**, 37 (1983).
[33]W. Hartl, H. Versmold, and U. Wittig, Ber. Bunsenges. Phys. Chem. **88**, 1063 (1984).
[34]T. Hashimoto, M. Shibayama, M. Fujimura, and H. Kawai, in *Block Copolymers: Science and Technology*, Vol. 3 of *Michigan Molecular Institute Symposium Series*, edited by D. J. Meir (Harwood Academic, Chur, Switzerland, 1983).
[35]T. Hashimoto, H. Tanaka, and H. Hasegawa, Macromolecules **18**, 1864 (1985).
[36]N. Ise and K. Ito (unpublished).
[37]N. Ise, T. Okubo, M. Sugimura, K. Ito, and H. J. Nolte, J. Chem. Phys. **78**, 536 (1983).
[38]When the interparticle distance was measured by the microscopic method, it was found to be smaller than $2D_0$ for highly charged latex particles at low concentrations, as discussed in review articles (Refs. 5–7). This situation required us to accept the existence of a substantial attractive interaction between latex particles through the intermediary of counterions. This attraction, together with the repulsive interaction between the particles *per se*, would form a secondary minimum. When the particles are not highly charged, the attraction is not intensive because the number of mediating counterions is correspondingly small. The particles are then located as far apart as possible from each other, namely at an average distance of $2D_0$. In other words, $2D_{\text{expt}} \simeq 2D_0$ for such low-charge-density particles. The latex samples, which are discussed in Figs. 11–14, have low charge numbers so that the equality relation mentioned in the text, $a_n \simeq 2D_0$ is reasonable.